Received: 11 February 2021 | Revised: 27 May 2021 | Accepted: 9 June 2021

DOI: 10.1111/ijag.16292

INTERNATIONAL JOURNAL OF Applied Glass SCIENCE

SPECIAL ISSUE ARTICLE

Polymer (PCL) fibers with Zn-doped mesoporous bioactive glass nanoparticles for tissue regeneration

Zuzana Neščáková[1] | **Hana Kaňková**[1] | **Dagmar Galusková**[1] | **Dušan Galusek**[1,2] | **Aldo R. Boccaccini**[3] | **Liliana Liverani**[3]

[1]Centre for functional and surface-functionalized glass, A. Dubček University of Trenčín, Trenčín, Slovakia

[2]Joint Glass Centre of the IIC SAS, TnUAD, FChPT STU, Trenčín, Slovakia

[3]Department of Materials Science and Engineering, Institute of Biomaterials, University of Erlangen-Nuremberg, Erlangen, Germany

Correspondence
Liliana Liverani, Institute of Biomaterials, Department of Materials Science and Engineering, University of Erlangen-Nuremberg, 91058 Erlangen, Germany.
Email: liliana.liverani@fau.de

Funding information
VEGA, Grant/Award Number: VEGA 1/0191/20; European Union's Horizon 2020, Grant/Award Number: 739566; European Regional Development Fund

Abstract

Composite fibrous membranes based on poly(ε-caprolactone) (PCL) and mesoporous bioactive glass nanoparticles (MBGNs) were fabricated by electrospinning. MBGNs and Zn-doped MBGNs prepared by microemulsion sol–gel method were successfully incorporated inside the polymeric fibers of 240 and 385 nm in diameter for undoped and Zn-doped PCL_MBGNs fibers, respectively. Thermal analysis showed that the concentration of MBGNs reached a maximum of around 21 wt% for Zn-doped MBGNs. Both PCL_MBGNs and PCL_MBGNs_Zn composite membrane exhibited bioactivity after immersion in simulated body fluid (SBF). X-ray diffraction (XRD) and Fourier transform infrared spectroscopy (FTIR) showed the evolution of composite membranes, confirming the formation of hydroxyapatite (HAp). However, the degradation products of membranes did not affect the viability and proliferation of murine stromal cells (ST-2) and thus the new fiber structures represent a suitable environment for cell adhesion. Therefore, the incorporation of mesoporous glass nanoparticles doped with therapeutically active Zn^{2+} ions inside the PCL fibers offers the possibility to create a multifunctional biomaterial suitable for drug delivery and tissue engineering.

KEYWORDS

benign solvents, composite fibers, composites, electrospinning, mesoporous bioactive glass nanoparticles, poly(ε-caprolactone), tissue engineering, zinc

1 | INTRODUCTION

Bioactive glass (BG)/polymer composites represent a wide group of biomaterials, where the advantages of both components are combined, leading to the creation of materials with enhanced properties suitable for several applications.[1,2] The use of bioactive glass particles in composites contributes to enhancing the functionality of polymers by inducing hydrophilicity and bioactivity in addition to improving the mechanical properties.[3,4] The polymeric component allows the formation of different structures exploiting standard polymeric processing techniques. The combination of polymers and bioactive glass leads also to modification of the biodegradability of the polymer matrix, which is of importance for applications in tissue engineering and drug delivery.[2,3,5,6] Individually, organic and inorganic materials may have different disadvantages, but when combined, the synergistic effect of both components can be exploited to enhance

the properties of the composite.[2,5] The combination of polymers and bioactive glasses may take various forms such as coatings, scaffolds, or dispersion of bioactive glass particles in polymeric fibers. In particular, bioactive materials can be trapped into polymeric fibers, without internalization, or can be loaded inside the fibers which can have a different diameter range, from micrometers to nanometers,[7] and be aligned or randomly assigned. Secondary configurations such as porous fibers, hollow and core-sheath structures can create multilayer meshes, membranes, cotton-like materials, etc.[6–8] The key motivation is to generate the so-called fourth-generation biomaterials, that besides biocompatibility, bioactivity and biodegradation include also biomimetic features. These biomaterials mimic natural´s hierarchical structures and mechanisms. In particular for tissue engineering, the aim is to reproduce a microstructure similar to the extracellular matrix (ECM), composed of micro and nanosized pores and fibers, which create a microenvironment with biochemical and structural support for cells.[9] For this purpose, fibrous structures can be obtained by the widely used, cost-effective, and versatile electrospinning technique (ELS). By ELS, a variety of materials, including biodegradable, nondegradable, synthetic, or natural polymers, can be processed making it attractive for bioengineering.[6] Different structures, compositions, and morphologies allow the use of these composites for regeneration and healing of hard tissue (bone,[10] cartilage[11]), soft tissue (vascular,[12] neural,[13] ocular, spinal cord), as well as for skin and wound healing.[14] Poly-ε-caprolactone (PCL) is one of the most used synthetic polymers in biomedical applications. PCL is a semicrystalline polyester, produced by relatively cheap ring-opening polymerization, highly processable due to its solubility in several organic solvents and low melting temperature (55–60°C),[15] and biodegradable by hydrolytic degradation within 2–3 years.[16,17] PCL has several advantages, however, its cell stimulation is weak. Fibrous structures offer suitable conditions for cell attachment and ingrowth, but the majority of polymers, including PCL, exhibit limited ability to stimulate cellular activity.[18] This is the reason for the preparation of composites combining PCL with materials providing bioactivity.[19] It has been shown that ionic degradation products of BGs such as silicon (Si) usually as silicic acid,[20] calcium (Ca), phosphorous (P), and other ions (Zn^{2+}, Cu^{2+}, Co^{2+}, Sr^{2+}, Ag^{2+}, etc.) lead to favorable intracellular and extracellular response.[20,21] Besides this, BGs enhance interaction with living tissue which results in the formation of chemical bonds via the formation of a hydroxycarbonate apatite (HCA) layer on BG surfaces in contact with biological fluids.[22] Significant progress in the development of BGs is represented by mesoporous bioactive glasses (MBGs), whose discovery[23] brings enormous possibilities for their biomedical application.[24] Compared to nonmesoporous BGs, MBGs exhibit higher specific surface area, pore-volume, bioactivity, and, in some cases, superior cytocompatibility.[25] Moreover, in comparison to conventional micrometer-sized BGs, nanosized MBGs exhibit interaction with cells at the nanoscale and a greater extent of integration with the extracellular matrix.[26] The reduced size of MBGs in the nanoscale allows their favorable use in composites, dental fillers, drug delivery systems, bioactive coatings, and scaffolds.[25] Besides the ions embedded in the MBGs structure, which provide therapeutic effects during the glass dissolution, pores can be also loaded with drugs and different kinds of biomolecules, thus making MBGs versatile carriers. Among the above-mentioned ionic degradation products, Zn^{2+} ions are attracting interest and zinc-based biomaterials have been increasingly investigated in recent years.[27,28] Mesoporous silica nanoparticles doped by zinc were produced as a tunable biodegradable platform for target therapy of breast cancer.[29] Zinc has desirable properties for tissue regeneration and therapy, plays a crucial role in osteogenesis,[30] is involved in homeostasis, angiogenesis, and has antibacterial, antifungal, and anticancer effects.[31] It is also strongly connected with skin and wound healing processes.[32] This work aims to incorporate MBG nanoparticles (MBGNs) and MBG nanoparticles doped with Zn (MBGNs_Zn) into PCL fibers fabricated by the electrospinning technique. The synthesis and characterization of particles were previously described by the authors.[33] The size of MBGNs allows the fabrication of electrospun PCL nanofibers, which may mimic the ECM morphology. The influence of the incorporation of MBGNs and MBGNs_Zn on fibers morphology, average diameter, and ion release profile from the composites was analyzed. Furthermore, possible cytotoxicity and the *in vitro* mineralization of the composite fibers were investigated.

2 | MATERIALS AND METHODS

2.1 | Bioactive glass nanoparticles synthesis

MBGNs based on the binary system composed of 90 mol% SiO_2 and 10 mol% CaO were synthesized via microemulsion sol–gel method.[34] To add subsidiary biological function, MBGNs were doped with Zn^{2+} ions, and MBGNs_Zn of 84 mol% SiO_2, 8 mol% CaO, and 8 mol% ZnO composition were processed according to the previous protocol developed by the authors.[33] Briefly, hexadecyltrimethylammonium bromide (CTAB) was dissolved in deionized water with the later addition of ethyl acetate. After hydrolysis of silica precursor, tetraethyl orthosilicate (TEOS), an adequate amount of the other precursors as $Ca(NO_3)_2 \cdot 4H_2O$ and $Zn(NO_3)_2 \cdot 6H_2O$ was added to the mixture. After the synthesis, the precipitate was washed, collected, and dried in an oven at 60°C for 24 h. Finally, the dried materials were calcined at 700°C for 2 h following a heating rate of 2°C min^{-1}.

2.2 | Electrospinning of fiber membrane

The solution for electrospinning was prepared from PCL (80 kDa, Sigma Aldrich) and a glacial acetic acid (AcOH) (VWR) used as a benign solvent.[35] Based on the protocol developed by Liverani et al.[35] PCL (20 wt%) was dissolved in an AcOH by stirring at room temperature overnight and put in an ultrasonic bath for 1h before the electrospinning process. To produce composite fibers, MBGNs and MBGNs_Zn (30 wt% respect to PCL), samples labeled as PCL_ MBGNs and PCL_ MBGNs_Zn, respectively, were added to the as-prepared PCL solution and dispersed by an ultrasonic homogenizer. These solutions were immediately electrospun by a single jet electrospinning apparatus (Starter Kit 40KV Web, Linari Engineering) under ambient conditions. The optimized electrospinning parameters for both composites were an applied voltage at 20 kV, tip-target distance of 11 cm, and a flow rate of 0.4 ml/h. Temperature and relative humidity were in the range of 22.5–24.5°C and 20%–30%. The fibers were collected on an aluminum foil and then stored for further investigations.

2.3 | Characterization

The structure and morphology of the fiber mats were observed with a scanning electron microscope (SEM; Auriga Base, Zeiss). Before SEM analysis samples were sputtered with gold using Sputter Coater (Q150T, Quorum Technologies Ltd.). The average diameter of the fibers was analyzed by measuring a diameter of 200 random fibers from SEM images. A software for SEM experimental control and analysis Gatan Microscopy Suite Software (GMS; Gatan Inc., AMETEK) was used to determine fiber diameter distribution. Further structural analysis was performed by Fourier Transform Infrared Spectroscopy (FTIR; IRAffinity-IS, Shimadzu) in attenuated total reflectance (ATR) mode, using a wavenumber range of 4000 to 400 cm^{-1} with a resolution of 4 cm^{-1} with 32 spectral scans. X-ray diffraction (XRD) patterns of the fiber mats were obtained using an X-ray diffractometer (MiniFlex 600, Rigaku) in the 2θ range of 10° to 80° equipped with Cu Kα radiation. A step size of 0.02° and dwell time of 1° per minute were used. To determine the wettability of fiber mats, the static contact angle was measured using a drop shape analyzer DSA30 (Krüss GmbH). Five samples were examined by the sessile drop method, in air atmosphere and room temperature, average values were reported. Thermogravimetry/Differential Thermal Analysis (TG/DTA) was performed to define weight loss during heat treatment of fibrous mats. Samples (5.8 mg) were decomposed in alumina crucibles in a controlled atmosphere of N_2/O_2. The TG/DSC measurements were carried out in the temperature range between 35 and 800°C at the heating rate of 3°C/min in the air using the Netzsch STA 449 F1 Jupiter simultaneous thermal analyzer (Erich NETZSCH GmbH & Co. Holding KG.). The TG/DSC records were evaluated by the Netzsch Proteus software.

2.4 | Determination of ion release

Fiber membranes were cut to an area of 1 cm^2 and immersed in 5ml of simulated body fluid (SBF), freshly prepared according to the protocol of Kokubo et al.[36] The samples were incubated at 37°C with an agitation speed of 120 rpm. At each predetermined time point (1, 3, 7, 14, and 21 days), the supernatant was sampled and 65% HNO_3 (TraceMetal Grade) was added to meet pH ≤ 2 to stabilize the solution containing the dissolved ions. The elemental analysis of the solution was carried out by optical emission spectroscopy with inductively coupled plasma (ICP-OES; Agilent 5100 SVDV, Agilent Technologie, Inc.). A series of four calibration solutions in the range 10–100 mg/L (Si), 50–150 mg/L (Ca), and 1–25 mg/L (Zn) were prepared to obtain a linear correlation between the signal intensity and concentration of ions. The reference standards certified for ICP techniques were diluted to prepare the stock calibration solutions. To deal with non-spectral interferences, the internal standardization technique with scandium (10 mg/L) was used. The precision of the analysis for all required ions expressed as RSD% was below 5%. The average values including standard deviations from three replicates for each dissolved ion were reported.

2.5 | Acellular bioactivity

The acellular bioactivity of the electrospun composite fibers was evaluated by immersion in an SBF medium. Samples cut to an area of 1 cm^2 were immersed in 5 ml of SBF and incubated under continuous agitation (120 rpm) at 37°C. After 1, 3, 7, and 14 days, the samples were removed from the SBF medium, gently rinsed with deionized water, and dried. The pH of the remaining media was recorded. Furthermore, the samples were analyzed using SEM and FTIR. The phase compositions of the fibers were characterized by X-ray diffraction (XRD) analysis using a diffractometer (Miniflex 600 HR, Rigaku). Data were collected over a 2θ range from 20° to 60° with a step size of 0.02°.

2.6 | In vitro cell tests

Before cell experiments, electrospun fibrous mats were cut to a circular shape of 1cm diameter, fixed by using Cell Crown supports (Scaffdex, Sigma Aldrich) and disinfected for 1 h with UV light irradiation. Samples were then placed into cell

culture plates and rehydrated by a complete cell culture medium (CCM). As a CCM Dulbecco's Modified Eagle Medium (Gibco, Thermo Fisher Scientific) was used, containing 10% fetal bovine serum and 0.1 mg/ml of each Penicillin and Streptomycin (Gibco, Thermo Fisher Scientific). Direct cell test was performed using murine stromal cells (ST-2) purchased from the Leibniz-Institut DSMZ—German Collection of Microorganisms and Cell Cultures GmbH, Germany. ST-2 Cell lines were maintained in CCM at 37°C in a humidified atmosphere of 95% air and 5% CO_2. The cells were routinely subcultured by trypsinization (0.25% Trypsin-EDTA, Gibco, Thermo Fisher Scientific). Harvested cells were diluted at a density of 25.000/fibrous mat and in 100 µl of CCM were seeded directly on each rehydrated sample, incubated for 5 min to allow soaking and then filled with 1mL of CCM. Samples were incubated for 1, 3, and 7 days at 37°C in 5% CO_2. After the incubation period, cell viability was assessed by WST-8-assay (CCK-8 Kit, Sigma Aldrich). Water-soluble tetrazolium salt, WST-8, is reduced by mitochondrial dehydrogenases to an orange formazan product. After incubation for 4 h at 37°C, the reaction product was measured at 450 nm using a microplate reader (PHOmo Elisa reader, Autobio Diagnostics Co. Ltd.). The amount of formazan produced is directly proportional to the number of living cells in culture. To investigate cell adhesion and morphology, staining with Rhodamine Phalloidin (RP; ThermoFisher Scientific) and DAPI (ThermoFisher Scientific) was performed. After fixation and permeabilization of the adherent cells, RP (8 µl/ml) was added and incubated at 37°C for 1 h. Samples were thoroughly washed by PBS and dyed by DAPI (1 µl/ml). Washed samples were analyzed with a fluorescent microscope (Axio Scope A1, Zeiss). All measurements were performed in triplicates.

2.7 | Statistical analyses

All experiments were carried out at least in triplicate. Results are expressed as mean ± standard deviation (SD). Statistical evaluation was assessed by using one-way analysis of variance (ANOVA) with $p < 0.05$ considered significant.

3 | RESULTS AND DISCUSSION

3.1 | Compositional and microstructural characterization

The composition of prepared MBGNs and Zn-MBGNs nanoparticles was measured by X-ray fluorescence (XRF; Bruker S8 Tiger) and inductively coupled plasma optical emission spectroscopy (ICP-OES; Agilent 5100 SVDV) and the results were published in our previous article.[33] The molar compositions (re-calculated to oxides) of the prepared nanoparticles are summarized in Table 1. Due to the nature of sample preparation for the ICP OES measurements, the high content of SiO_2 could not be exactly measured by the method. Therefore, the value of Si content in the samples was obtained as normalized values to the sum 100%.

TABLE 1 Chemical composition of MBGNs and Zn-MBGNs determined by XRF and ICP-OES

Composition XRF (mol %)	MBGNs	Zn-MBGNs
SiO_2	90.0	83.2
CaO	10.0	8.4
ZnO	–	8.4
Composition ICP-OES (mol %)		
SiO_2	88.4	83.8
CaO	11.6	8.3
ZnO	–	7.9

SEM analysis of PCL_MBGNs and Zn-doped PCL_MBGNs fibers, reported in Figure 1A–D, shows a homogeneous fiber diameter distribution around 240 and 385 nm for undoped and Zn-doped PCL_MBGNs fibers, respectively. To obtain this distribution more than 500 fibers from different micrographs of both compositions were analyzed in different points of each fibrous mats. The obtained fiber diameter is comparable with previous results found in literature, where PCL average fiber diameter for neat PCL mats in a range of 110–3850 nm have been reported.[37,38] These results are also similar to those obtained by the authors for PCL and PCL_ BGs fibers with 30 wt% of BGs, with a fiber diameter at around 175 and 375 nm, respectively. Moreover, the addition of MBGNs led to an increase of fiber diameter, resulting from the higher viscosity of the spinning solution.[39]

According to the reported results, we can conclude that the Zn incorporation in bioactive glass particles did not influence significantly the average fiber diameter but, on the other hand, it contributed to increasing the diameter distribution range up to 1.4 µm.

A detailed magnified SEM micrograph shown in Figure 2 displays the distribution of the MBGNs_Zn particles inside the polymeric fiber. Glass particles tend to form clusters alongside the fibers, MBGNs are not well dispersed in the solution and as a result, they are not stabilized in that solution. This effect could be explained by the incorporation of a high concentration of bioactive glass particles, close to 30 wt% with respect to PCL, that affects the viscosity and conductivity of the solution, causing ulterior agglomeration.

3.2 | Thermal characterization and contact angle measurement

The thermal evolution and decomposition of PCL fibers were determined by TG-DTA, carried out in an oxygen

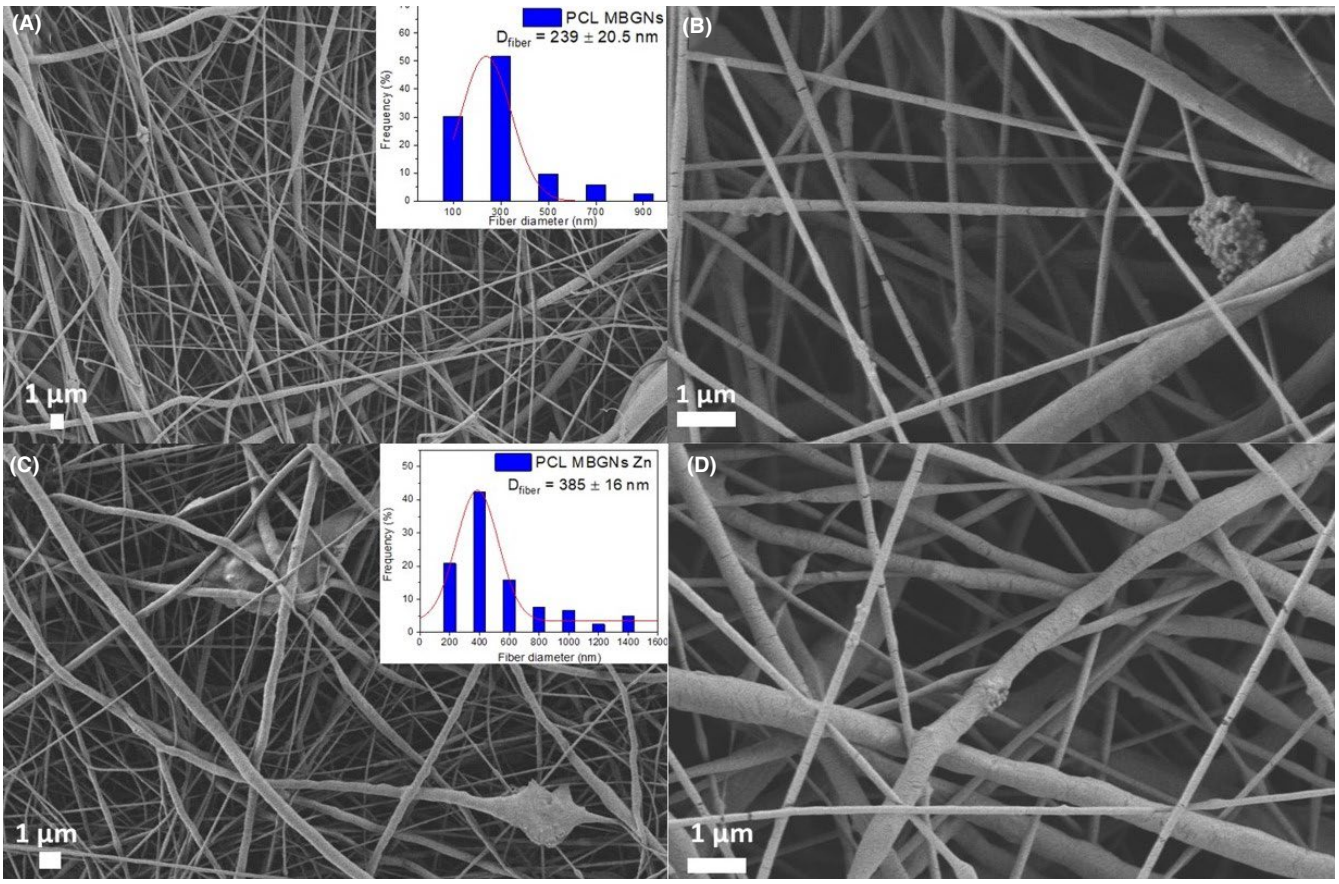

FIGURE 1 SEM micrographs of electrospun fibers (A, B) PCL_MBGNs and (C, D) PCL_MBGNs_Zn. (B) and (D) show magnified images of the studied fibers. Insets on (A) and (D) show the fibers diameter distribution

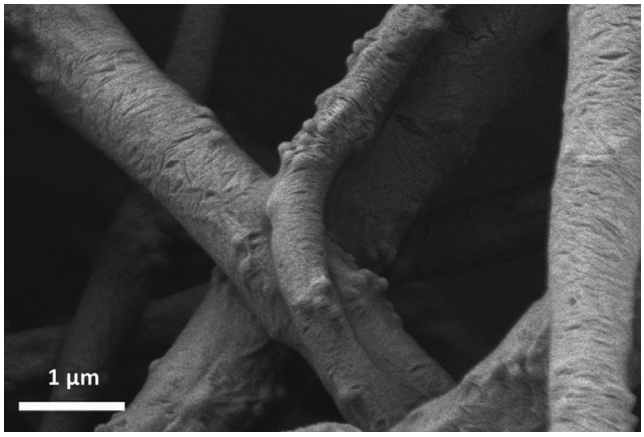

FIGURE 2 Detailed magnified SEM micrograph of electrospun Zn-doped PCL_MBGNs fibers

atmosphere, as shown in Figure 3. As indicated in previous works, PCL shows only one thermal degradation between 300 and 420°C with a significant weight loss, reaching values of 86.5% and 79.15%, for undoped and Zn-doped MBGNs, respectively.[40,41] Thus, MBGNs were incorporated inside the fibers in an amount of ~14 and ~21 wt%, for MBGNs and MBGNs_Zn, respectively. Mass loss is significantly lower than in previous results obtained in similar systems[42] and it could be related to the more effective incorporation of the MBGNs that finally are embedded in the PCL fibers.

Moreover, in the case of undoped MBGNs, this weight loss was accompanied by the typical exothermic peak for PCL fibers with a maximum at around 378°C. This peak indicates the maximum degradation rate of the sample reached at that temperature.[14] The most intense peak is shown to be split into three peaks indicating that the thermal degradation of PCL occurred above 310°C in three steps. This effect is associated with the decomposition of PCL in CO_2, CO, water, and short-chain acids.[43] The existence of these three peaks is characteristic for the decomposition of PCL in an oxygen atmosphere.

In addition to the thermal characterization, the hydrophobic nature of these materials was also analyzed as shown in Figure 4. To determine this property, the contact angle was measured. A change in the values of the contact angle gives information about how effective is the surface modification of the fibers, mostly in terms of porosity and roughness.[44]

Since the measured values for contact angle were 100, 107, and 93° for PCL, PCL_MBGNs, and PCL_MBGNs_Zn, respectively, no significant difference among them was detected. Thus, it seems that the MBGNs incorporated in

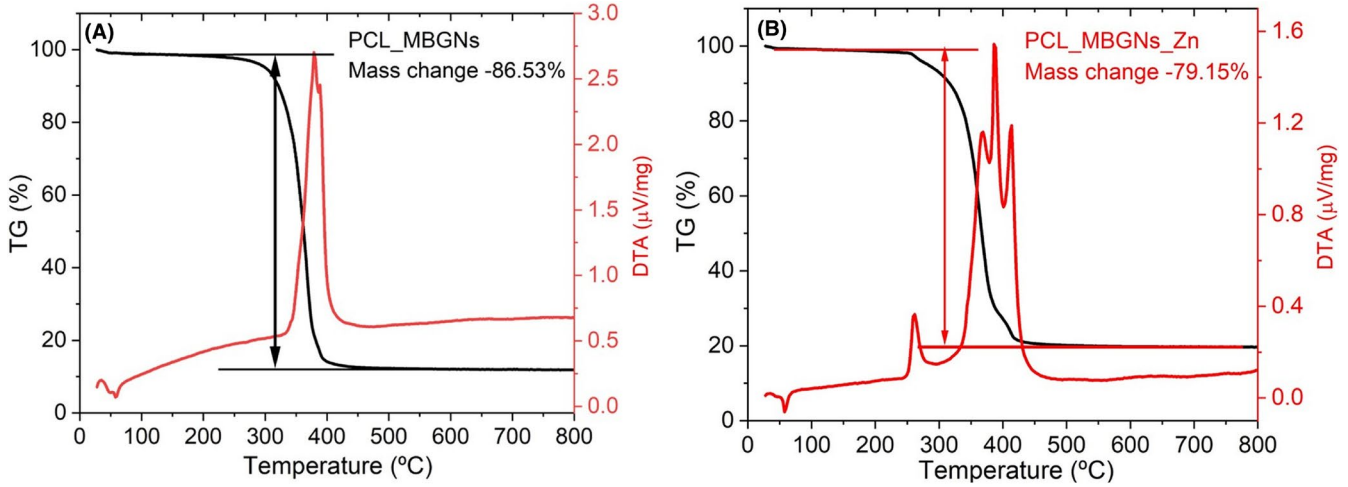

FIGURE 3 TG-DTA of PCL_MBGNs (A) and Zn-doped PCL_ MBGNs_Zn (B)

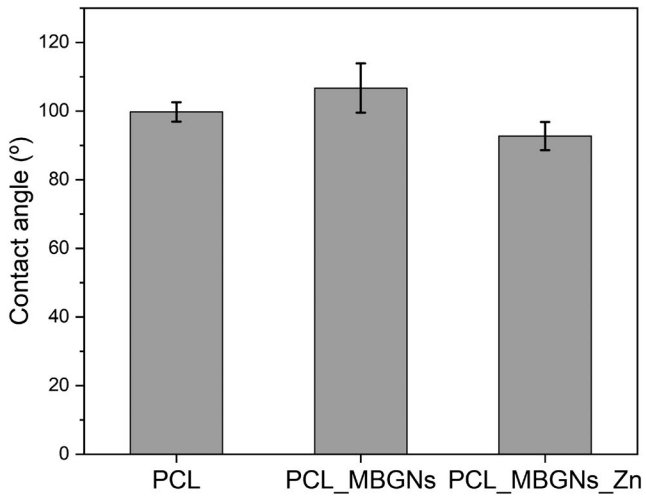

FIGURE 4 Contact angle of PCL, PCL_MBGNs, and Zn-doped PCL_MBGNs fiber mats

the PCL matrix do not affect the hydrophobic behavior of PCL electrospun fiber mats. Moreover, most of the obtained values are in the 98–110° range that has been previously reported by Sant et al.[45]

3.3 | Acellular bioactivity of electrospun composite fibers

The bioactivity of a material is determined as the ability to react with aqueous media, resulting in ion release and precipitation of biomimetic apatite layer.[46] This layer represents an interface between the substrate and host tissue and is crucial for consequential cell adhesion and tissue regeneration. The simulated body fluid (SBF) developed by Kokubo et al.[47] mimics the inorganic composition of human blood plasma and is considered as a standard solution for immersion test and bioactivity determination.[36,48] Bioglass® 45S5, as a representative of highly bioactive material, forms hydroxyapatite—$Ca_{10}(PO_4)_6(OH)_2$ (HAp) within a few hours after immersion in SBF.[49] The formation of HAp is described by a series of surface reactions which start with a rapid exchange of Ca^{2+} with protons, followed by the breakdown of the silica network and formation of silica-rich layer. Migration and precipitation of Ca^{2+} and PO_4^{3-} ions on this layer lead to the creation of amorphous calcium phosphate (CaP) which by incorporation of anions forms a crystalline (usually carbonate) apatite.[50] The SEM micrographs in Figure 5 show electrospun membranes after soaking in SBF and the morphological changes connected with HAp formation. On days 1, 3, and 7, no morphological changes associated with mineralization were observed (Figure 5A,B), however, some surface changes appear to have occurred. Complete degradation of PCL is usually quite long, thus PCL is used mainly in the replacement of hard tissue where the healing process takes an extended period of time.[16] In this case, possible faster degradation may occur as MBGNs are covered by a thin layer of the polymeric matrix and can interact with SBF directly. Degradation of PCL/PGS fibers via surface erosion in a similar time range was described also by Luginina et al.[51] In this work, rosettes of HAp are visible on the electrospun membranes after 14 days of immersion (Figure 5D), however, a compact HAP layer is still not visible. The rate of HAp formation is similar to the one reported by Sergi et al.,[42] who pointed out that rapid bioactivity is not of pivotal importance for specific applications in soft tissue engineering, for example, wound dressing, as opposed to bone tissue engineering.

FTIR and XRD analyses were performed to examine the evolution of the structure and chemical composition of the prepared fiber mats after soaking in SBF solution from 1 to 14 days. The results are shown in Figure 6.

The XRD patterns of all PCL_MBGNs and PCL_ MBGNs_Zn composites exhibit characteristic PCL

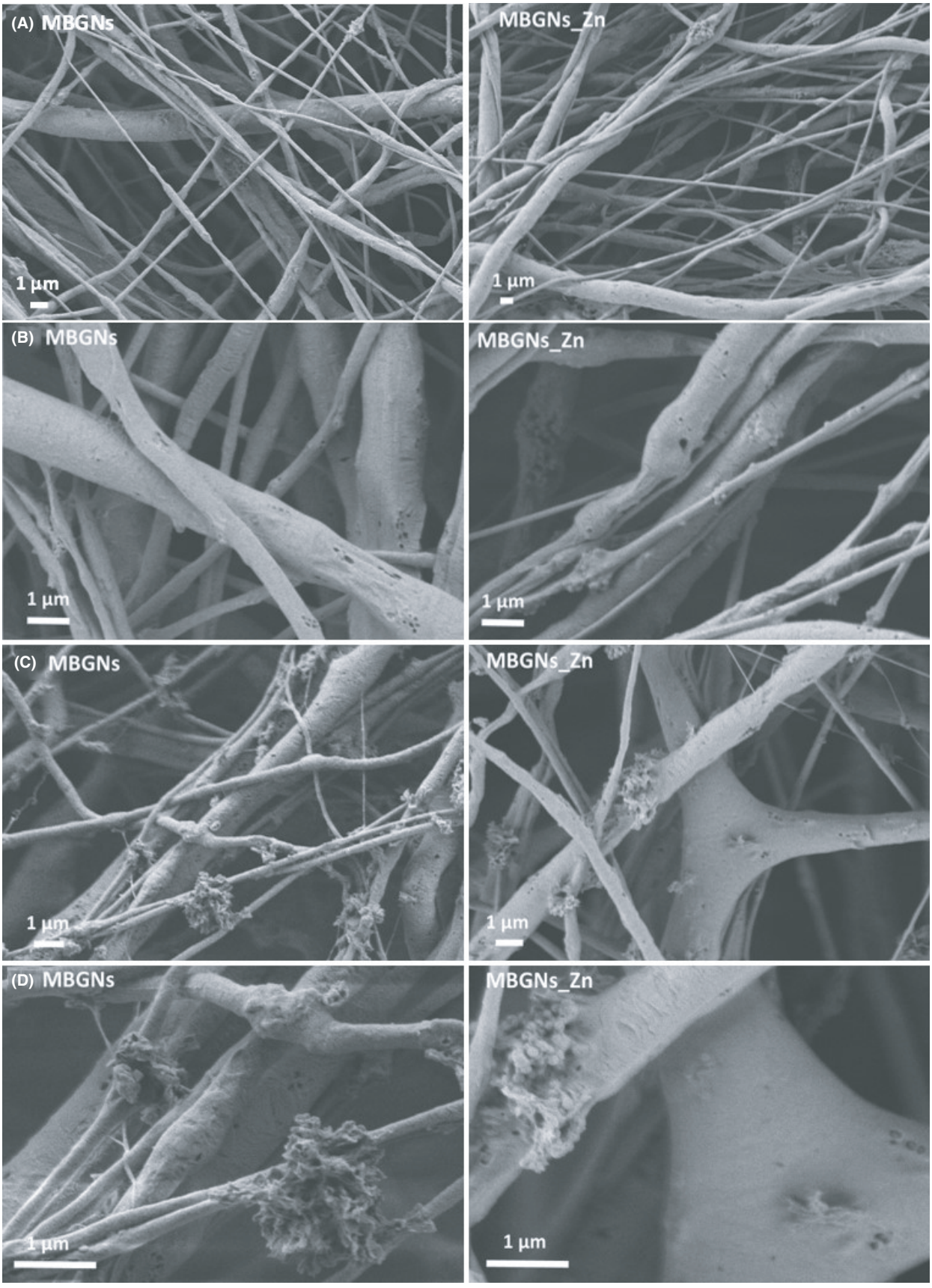

FIGURE 5 SEM micrographs of PCL_MBGNs (left) and PCL_MBGNs_Zn (right) composite membranes after immersion in SBF for (A) 3 days, (B) 7 days, (C) 14 days, (D) higher magnification of (C)

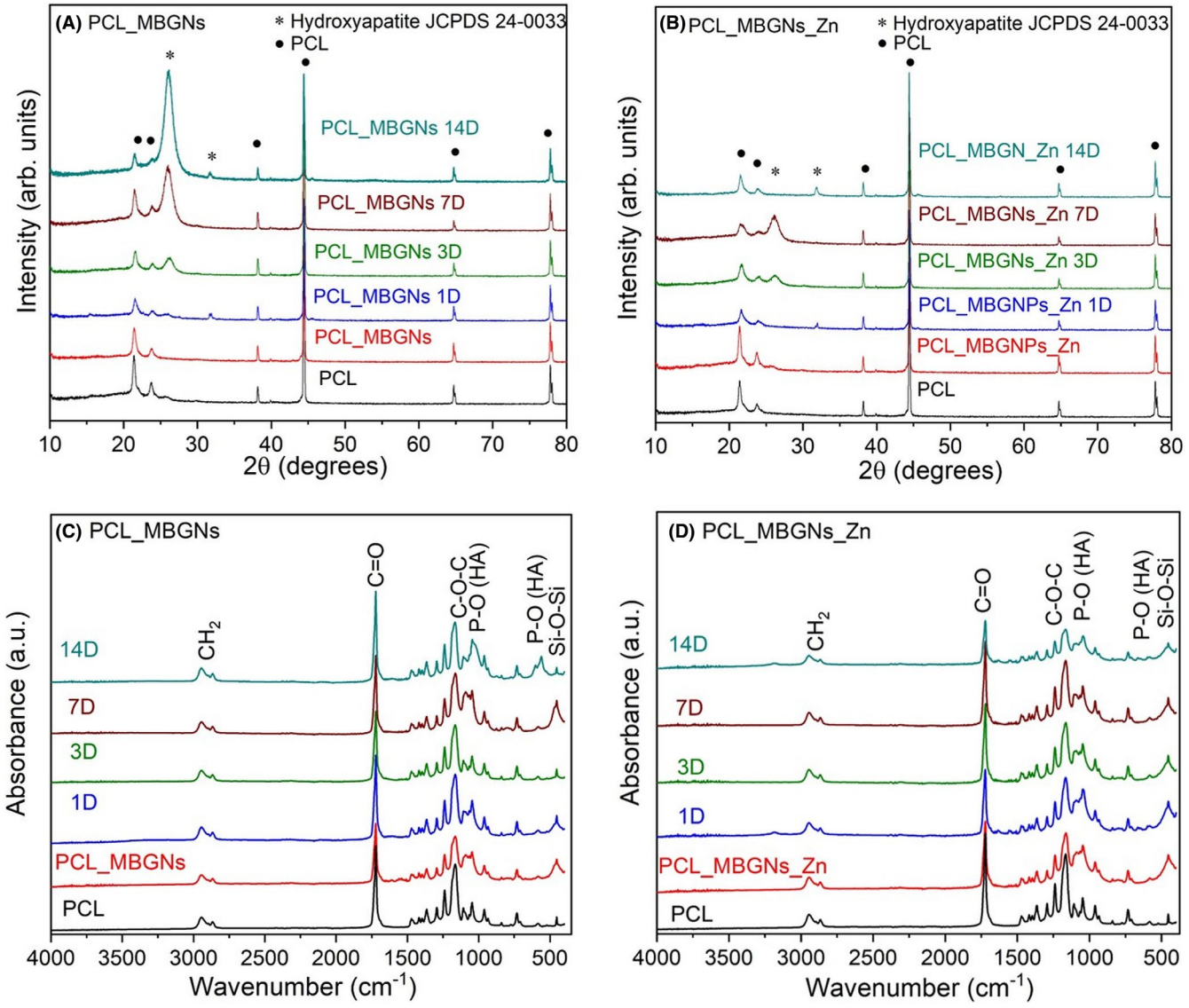

FIGURE 6 XRD diffraction patterns of PCL_MBGNs (A) and PCL_MBGNs_Zn (B) fiber mats before and after soaking in SBF solution. (C) and (D) FT-IR spectra of PCL_MBGNs and PCL_MBGNs_Zn under the same conditions

diffractions with two additional diffraction maxima at $2\theta = 26.2°$ and $2\theta = 31.6$, which are attributed to the presence of HA (JCPDS file 24-0033).[52] The figures show an increased intensity trend for the $2\theta = 26.8°$ diffraction, corresponding to the (002) crystalline direction, with the soaking time in SBF instead of the most intense peak described in the JCPDS file 24-0033 for crystalline HA, at around 31.6°. This effect could be attributed to the existence of preferential orientation of the HA crystals in the fibers. Moreover, as it was indicated previously, similar behavior is observed for Zn-doped PCL_MBGNs. However, the diffraction maxima corresponding to HA crystalline phase for the different soaking times are less intense with respect to the corresponding ones of undoped composite samples, indicating that the presence of Zn^{2+} ions has delayed the formation of HAp.

FTIR spectra in Figure 6C,D of PCL, PCL_MBGNs, and Zn-doped PCL_MBGNs before and after soaking in SBF solution confirm the behavior observed in XRD diffraction patterns. The spectra before this immersion in SBF solution exhibit the characteristic PCL bands observed previously by other authors[53,54]: 2942, 2865, and 1366 cm^{-1}, that are associated to stretching of CH_2 alkyl group; 1722 cm^{-1}, related to carbonyl C=O stretching and 1240 and 1165 cm^{-1} peaks, attributed with symmetric and asymmetric C–O–C stretching, respectively; finally, the peak at 1294 cm^{-1} associated to the backbone C–O and C–C stretching. Finally, the peaks at around 450 cm^{-1} are associated to Si–O–Si of amorphous silicate glasses.[55]

The FTIR spectra measured at different times after soaking in SBF solution showed the bands that correspond to the HAp layer: that is, P–O bending vibration at around

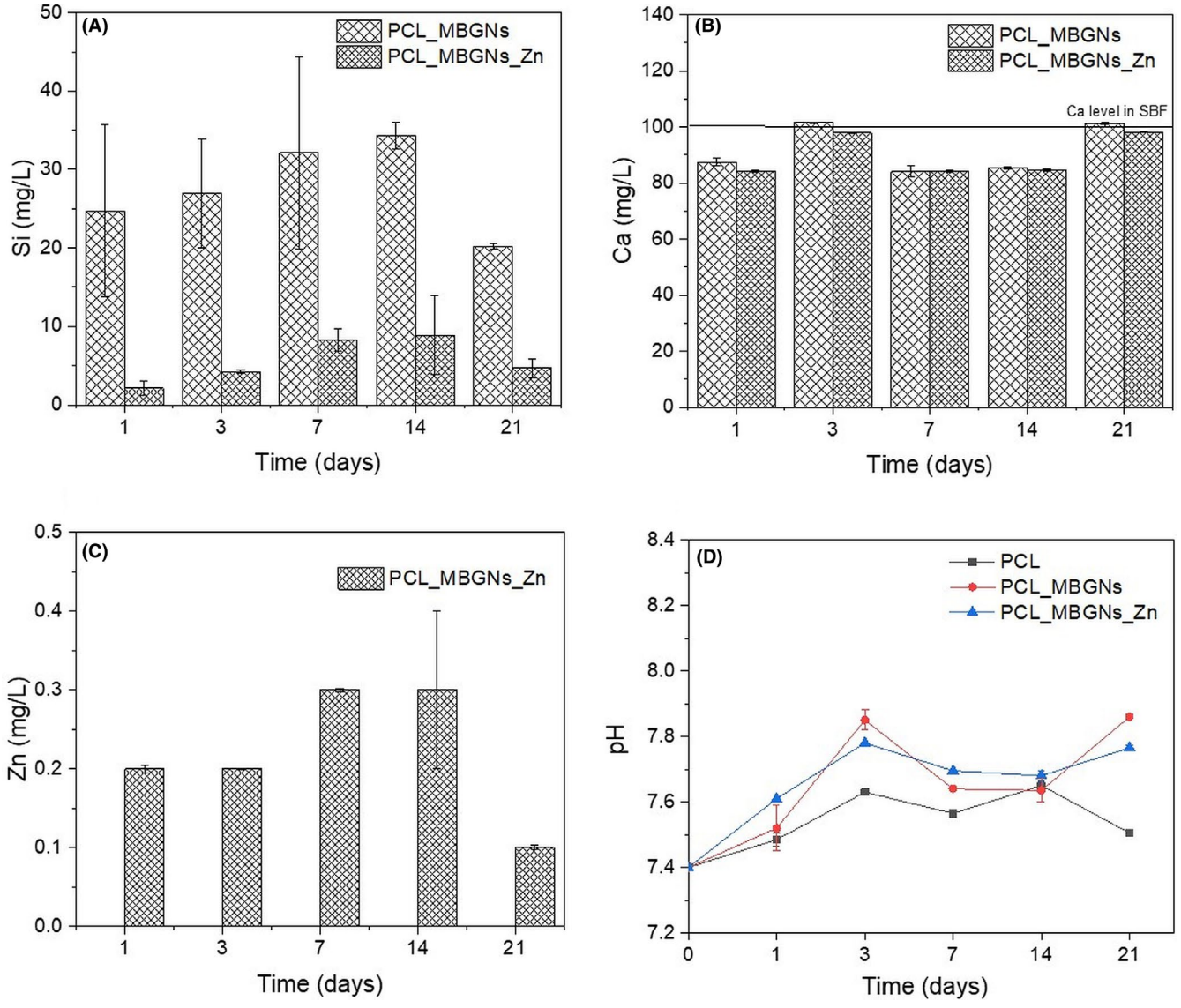

FIGURE 7 The concentration of Si (A), Ca (B), and Zn (C) in SBF and its pH (D) during incubation with PCL-MBGNs and PCL_MBGNs_Zn fibers

600 cm^{-1} and the P–O asymmetric stretching vibration at around 1030 cm^{-1} that indicated the formation of HAp on fiber.[55] It was observed that the P–O asymmetric stretching vibration was detected 7 days after immersion of PCL_MBGNs in SBF solution (Figure 6C). Furthermore, the P–O bending vibration at 600 cm^{-1} is observed at 14 days after immersion in SBF, while it is slightly observed in the Zn-doped PCL_MBGNs. It means that the Zn^{2+} ions cause a delay in the HAp formation and thus the bioactivity of the Zn-doped samples is lower. It is well-known that ZnO could behave both as a network modifier but also as an intermediate oxide and according to this, ZnO partially replaces the CaO forming ZnO_4^{2-} species which require Ca ions for charge balancing. The effect is increased due to the high content of Zn dopant. Thus, the amount of Ca^{2+} ions available for the formation of HAp is even smaller. Therefore, the glass dissolution decreases and as a consequence the HAp formation is delayed.[56,57]

In order to better understand the degradation of the composite membranes, the compositional change of SBF in time was evaluated by ICP-OES. Ca, Si, and Zn related to the glass dissolution process were determined in the horizon of 21 days and are shown in Figure 7A–C. An increase in Si concentration in SBF after 1 day of immersion confirms a dissolution of glass particles in composite membranes. MBGNs dissolve faster compared to Zn-doped MBGNs. These results are consistent with the statement of Atkinson et al.[58] who described that the samples with higher content of zinc (5 mol%) show a slower dissolution process, so its durability is increased. Zn^{2+} ions may, respectively, act as a network modifier and network former and may reduce the glass dissolution[59] as was already mentioned. The amount of zinc released to the SBF solution

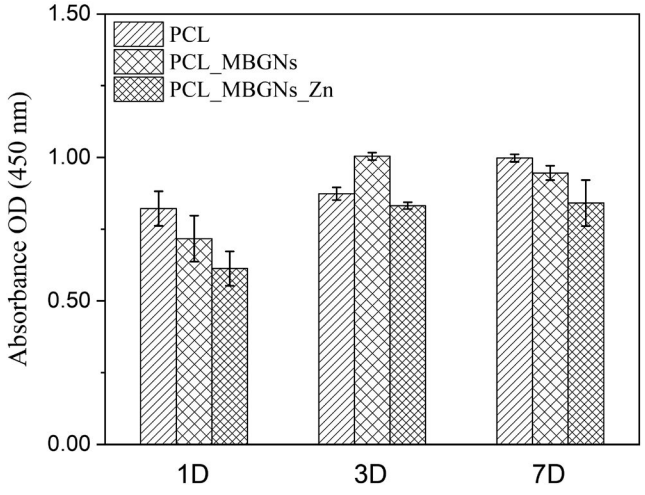

FIGURE 8 Cell viability of ST-2 cells determined by WST-8 assay (OD 450 nm) after direct seeding of cells on PCL and PCL_MBGNs, PCL_MBGNs_Zn electrospun fibers

is low (Figure 7C), which supports the assumption of the durability of the Zn-doped glass. The other explanation for a lower amount of Zn in SBF, could be the reaction of Zn^{2+} with PO_4^{3-} and its incorporation into a new crystalline phase, hopeite $Zn_3(PO_4)_2{\cdot}4H_2O$.[30] The process of biomineralization is also supported by the data displayed in Figure 7B reporting the presence of Ca in SBF medium. The detected concentration of Ca is comparable or lower than the concentration of calcium in SBF, which could be explained by its incorporation into $Ca_5(PO_4)_3(OH)$.

The pH of the supernatant SBF was measured (Figure 7D) and the increased pH value in the case of PCL_MBGNs and PCL_MBGNs_Zn composites confirmed the degradation of membranes. Degradation products as a result of glass dissolution lead to an increase in pH values. However, the changes are still in a range which is suitable for cell culture without the need for pretreatment.

3.4 | Cytocompatibility evaluation

Cytocompatibility of membranes was tested in direct contact with murine stromal cells ST-2. Viability was tested using WST-8 method, based on mitochondrial activity. The effect of direct contact of cells with the material on cell survival and proliferation was evaluated. Figure 8 shows viable cells seeded on the surface of the membrane for 1, 3, and 7 days. Compared to the control, represented by neat PCL fibers, there is no significant influence of MBGNs and MBGNs_Zn loading on cell viability and proliferation. Moreover, an increase in the number of cells over time was observed, which supports the cytocompatibility of the proposed materials. The results and optical density (OD) values are in accordance with the data published by Sergi et al.[42] who tested PCL fibers doped by Zn-doped bioactive glass prepared by the conventional melt-quenching route. It is important to mention that also fibers loaded by zinc-enriched MBGNs did not have a negative effect on cell growth. It is well-known that if zinc exceeds a certain concentration, it can have a cytotoxic effect. Vallet-Regi's group demonstrated that MBGs doped by 7 mol% ZnO were cytotoxic.[60] The amount of zinc that is considered nontoxic but still provides the required biological properties is 5 mol%.[61,62] We have already confirmed the cyto compatibility of the prepared MBGNs_Zn particles in our previous work, where the medium with dissolution products of the nanoparticles positively affected and increased the proliferation of MG-63 and MEF cell lines.[33] However, it should be emphasized that those were indirect tests with an elution extract while the direct contact of cells with the material is more challenging.[63] The composite membranes showed lower values of surviving cells compared to the PCL control but the number of viable cells was always above 70% of the control. The composites thus met the biocompatibility criteria of the ISO standard on the conditioned media.[64] The incorporation of MBGNs and MBGNs_Zn particles in PCL matrix slows down PCL degradation and associated ion release. This system suggests that slowing the release of compounds could promise a cell-safe environment suitable for long-term applications. This statement is also supported by the results obtained by fluorescent microscopy shown in Figure 9. A visible characteristic cellular morphology and a confluent monolayer of cells seeded on the membranes are visible. Cell morphology visualized by fluorescent staining of nuclei and cytoskeleton displays prolonged actin filaments corresponding to extended filopodia which have the role of sensing migration and cell–cell interaction.[65] Based on the above-mentioned results, the membranes are considered cytocompatible and can support cell adhesion.

4 | CONCLUSIONS

Polycaprolactone/mesoporous bioactive glass nanoparticle composite fibers were successfully fabricated by electrospinning using acetic acid as a benign solvent. MBGNs and MBGNs_Zn were incorporated inside the fibers with a final concentration of 14 and 21 wt% for MBGNs and MBGNs_Zn, respectively. Zinc incorporated in PCL_MBGNs_Zn composite slowed down the mineralization. However, both composite membranes, after immersion in simulated body fluid, formed hydroxyapatite (HAp) on their surfaces. Composite membranes showed limited degradation in an aqueous environment up to 14 days. The degradation products did not lead to any cytotoxic effect on murine stromal cells (ST-2). The fibrous nanostructure provided a suitable environment for cell adhesion and spreading. Therefore, these composite structures could be an attractive candidate for potential use as

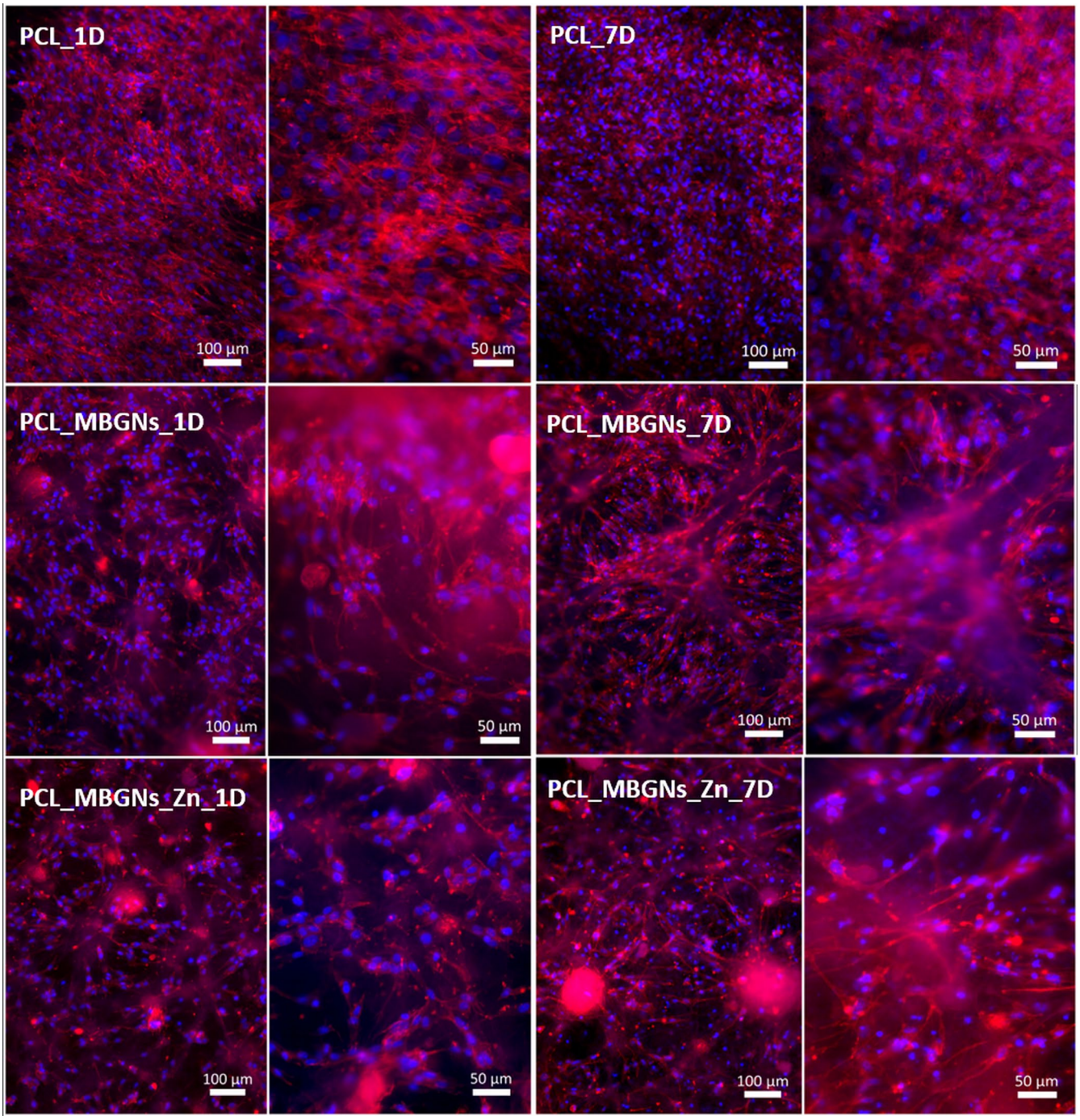

FIGURE 9 Fluorescent staining of adherent ST-2 cells on PCL and PCL_MBGNs, PCL_MBGNs_Zn composites after 1 and 7 days of incubation

drug delivery system as well as for therapy and regeneration of tissues.

ACKNOWLEDGMENTS

This paper is a part of the dissemination activities of the project FunGlass. This project has received funding from the European Union's Horizon 2020 research and innovation program under grant agreement No 739566. Publication was created also in the frame of project: Advancement and support of R&D for Centre for diagnostics and quality testing of materials in the domains of the RIS3 SK specialization, ITMS2014+:313011W442, based on the Operational Programme Integrated Infrastructure and funded from the European Regional Development Fund. ICP-OES measurements were carried out thanks to the grant VEGA 1/0191/20.

CONFLICT OF INTEREST

There are no conflicts to declare.

ORCID

Zuzana Neščáková https://orcid.org/0000-0001-9140-450X
Hana Kaňková https://orcid.org/0000-0001-5494-9754
Dagmar Galusková https://orcid.org/0000-0003-4114-1048
Dušan Galusek https://orcid.org/0000-0001-5995-8780
Aldo R. Boccaccini https://orcid.org/0000-0002-7377-2955
Liliana Liverani https://orcid.org/0000-0002-4270-4861

REFERENCES

1. Rezwan K, Chen QZ, Blaker JJ, Boccaccini AR. Biodegradable and bioactive porous polymer/inorganic composite scaffolds for bone tissue engineering. Biomaterials. 2006;27(18):3413–31.
2. Zambanini T, Borges R, Marchi J. Bioactive glass/polymer composites for drug delivery. In: Kaur G, editor. Clinical Applications of Biomaterials. Cham: Springer International Publishing; 2017. p. 287–311.
3. Rizwan M, Hamdi M, Basirun WJ. Bioglass® 45S5-based composites for bone tissue engineering and functional applications. J Biomed Mater Res Part A. 2017;105(11):3197–223.
4. Huan Z, Zhou J, Duszczyk J. Magnesium-based composites with improved in vitro surface biocompatibility. J Mater Sci Mater Med. 2010;21(12):3163–9.
5. Barrioni BR, Aline A, De OR. Biocompatible glasses. Marchi J, editor. Biocompatible Glasses. Cham: Springer International Publishing. (Advanced Structured Materials; vol. 53); 2016. p. 1–17.
6. Doostmohammadi M, Forootanfar H, Ramakrishna S. Regenerative medicine and drug delivery: Progress via electrospun biomaterials. Mater Sci Eng C. 2020;109:110521.
7. Boccaccini AR, Erol M, Stark WJ, Mohn D, Hong Z, Mano JF. Polymer/bioactive glass nanocomposites for biomedical applications: a review. Compos Sci Technol. 2010;70(13):1764–76.
8. Syed MR, Khan M, Sefat F, Khurshid Z, Zafar MS, Khan AS. Bioactive glass and glass fiber composite: Biomedical/dental applications. Biomedical, Therapeutic and Clinical Applications of Bioactive Glasses. Elsevier Ltd.; 2018. p. 467–95.
9. Michel G, Tonon T, Scornet D, Cock JM, Kloareg B. Central and storage carbon metabolism of the brown alga *Ectocarpus siliculosus*: insights into the origin and evolution of storage carbohydrates in Eukaryotes. New Phytol. 2010;188(1):67–81.
10. Ghasemi-Mobarakeh L, Prabhakaran MP, Balasubramanian P, Jin G, Valipouri A, Ramakrishna S. Advances in electrospun nanofibers for bone and cartilage regeneration. J Nanosci Nanotechnol. 2013;13(7):4656–71.
11. Rajzer I, Dziadek M, Kurowska A, Cholewa-Kowalska K, Ziąbka M, Menaszek E, et al. Electrospun polycaprolactone membranes with Zn-doped bioglass for nasal tissues treatment. J Mater Sci Mater Med. 2019;30(7):80.
12. Awad NK, Niu H, Ali U, Morsi YS, Lin T. Electrospun fibrous scaffolds for small-diameter blood vessels: A review. Membranes. 2018;8(1):1–26.
13. Sun M, Downes S. Physicochemical characterisation of novel ultra-thin biodegradable scaffolds for peripheral nerve repair. J Mater Sci Mater Med. 2009;20(5):1181.
14. Zahedi E, Esmaeili A, Eslahi N, Shokrgozar MA, Simchi A. Fabrication and characterization of core-shell electrospun fibrous mats containing medicinal herbs for wound healing and skin tissue engineering. Mar Drugs. 2019;17(1):1–13.
15. Nair LS, Laurencin CT. Biodegradable polymers as biomaterials. Prog Polym Sci. 2007;32(8–9):762–98.
16. Malikmammadov E, Tanir TE, Kiziltay A, Hasirci V, Hasirci N. PCL and PCL-based materials in biomedical applications. J Biomater Sci Polym Ed. 2018;29(7–9):863–93.
17. Abedalwafa M, Wang F, Wang L, Li C. Biodegradable poly-epsilon-caprolactone (PCL) for tissue engineering applications: a review. Rev Adv Mater Sci. 2012;34:123–40.
18. Liu J, Kerns DG. Mechanisms of guided bone regeneration: a review. Open Dent J. 2014;8(1):56–65.
19. Hidalgo Pitaluga L, Trevelin Souza M, Dutra Zanotto E, Santocildes Romero M, Hatton P. Electrospun F18 bioactive glass/PCL—poly (ε-caprolactone)—membrane for guided tissue regeneration. Materials. 2018;11(3):400.
20. Obata A, Iwanaga N, Terada A, Jell G, Kasuga T. Osteoblast-like cell responses to silicate ions released from 45S5-type bioactive glass and siloxane-doped vaterite. J Mater Sci. 2017;52(15):8942–56.
21. Hoppe A, Güldal NS, Boccaccini AR. A review of the biological response to ionic dissolution products from bioactive glasses and glass-ceramics. Biomaterials. 2011;32(11):2757–74.
22. Hench LL, Splinter RJ, Allen WC, Greenlee TK. Bonding mechanisms at the interface of ceramic prosthetic materials. J Biomed Mater Res. 1971;5(6):117–41.
23. Yan X, Yu C, Zhou X, Tang J, Zhao D. Highly ordered mesoporous bioactive glasses with superior in vitro bone-forming bioactivities. Angew Chemie Int Ed. 2004;43(44):5980–4.
24. Baino F, Hamzehlou S, Kargozar S. Bioactive glasses: where are we and where are we going? J Funct Biomater. 2018;9(1):25.
25. Lalzawmliana V, Anand A, Roy M, Kundu B, Nandi SK. Mesoporous bioactive glasses for bone healing and biomolecules delivery. Mater Sci Eng C. 2020;106:110180.
26. Narayan R, Nayak UY, Raichur AM, Garg S. Mesoporous silica nanoparticles: a comprehensive review on synthesis and recent advances. Pharmaceutics. 2018;10(3):1–49.
27. Qu X, Yang H, Yu Z, Jia BO, Qiao H, Zheng Y, et al. Serum zinc levels and multiple health outcomes: Implications for zinc-based biomaterials. Bioact Mater. 2020;5(2):410–22.
28. Su Y, Cockerill I, Wang Y, Qin Y-X, Chang L, Zheng Y, et al. Zinc-based biomaterials for regeneration and therapy. Trends Biotechnol. 2019;37(4):428–41.
29. Chen S, Greasley SL, Ong ZY, Naruphontjirakul P, Page SJ, Hanna JV, et al. Biodegradable zinc-containing mesoporous silica nanoparticles for cancer therapy. Mater Today Adv. 2020;6:100066.
30. Balasubramanian P, Strobel LA, Kneser U, Boccaccini AR. Zinc-containing bioactive glasses for bone regeneration, dental and orthopedic applications. Biomed Glas. 2015;1(1):51–69.
31. Chasapis CT, Spiliopoulou CA, Loutsidou AC, Stefanidou ME. Zinc and human health: an update. Arch Toxicol. 2012;86(4):521–34.
32. Stubbs N, Lansdown ABG, Ågren MS, Mirastschijski U, Scanlon E. Zinc in wound healing: theoretical, experimental, and clinical aspects. Wound Repair Regen. 2007;15(1):2–16.
33. Neščáková Z, Zheng K, Liverani L, Nawaz Q, Galusková D, Kaňková H, et al. Multifunctional zinc ion doped sol – gel derived mesoporous bioactive glass nanoparticles for biomedical applications. Bioact Mater. 2019;4:312–21.
34. Liang Q, Hu Q, Miao G, Yuan B, Chen X. A facile synthesis of novel mesoporous bioactive glass nanoparticles with various morphologies and tunable mesostructure by sacrificial liquid template method. Mater Lett. 2015;148:45–9.

35. Liverani L, Boccaccini A. Versatile production of poly(epsilon-caprolactone) fibers by electrospinning using benign solvents. Nanomaterials. 2016;6(4):75.
36. Kokubo T, Takadama H. How useful is SBF in predicting in vivo bone bioactivity? Biomaterials. 2006;27(15):2907–15.
37. Liverani L, Killian MS, Boccaccini AR. Fibronectin functionalized electrospun fibers by using benign solvents: best way to achieve effective functionalization. Front Bioeng Biotechnol. 2019;7:1–12.
38. Kim HH, Kim MJ, Ryu SJ, Ki CS, Park YH. Effect of fiber diameter on surface morphology, mechanical property, and cell behavior of electrospun poly(ε-caprolactone) mat. Fibers Polym. 2016;17(7):1033–42.
39. Schuhladen K, Raghu SNV, Liverani L, Neščáková Z, Boccaccini AR. Production of a novel poly(ε-caprolactone)-methylcellulose electrospun wound dressing by incorporating bioactive glass and Manuka honey. J Biomed Mater Res Part B Appl Biomater. 2021;109(2):180–92.
40. Wan Y, Lu X, Dalai S, Zhang J. Thermophysical properties of polycaprolactone/chitosan blend membranes. Thermochim Acta. 2009;487(1–2):33–8.
41. Ma W, Yang X, Ma L, Wang X, Zhang L, Yang G, et al. Fabrication of bioactive glass-introduced nanofibrous membranes with multifunctions for potential wound dressing. RSC Adv. 2014;4(104):60114–22.
42. Sergi R, Cannillo V, Boccaccini AR, Liverani L. Incorporation of bioactive glasses containing Mg, Sr, and Zn in electrospun PCL fibers by using benign solvents. Appl Sci. 2020;10(16):5530.
43. Vogel C, Siesler HW. Thermal degradation of poly(ε-caprolactone), poly(L-lactic acid) and their blends with poly(3-hydroxybutyrate) studied by TGA/FT-IR spectroscopy. Macromol Symp. 2008;265(1):183–94.
44. Cipitria A, Skelton A, Dargaville TR, Dalton PD, Hutmacher DW. Design, fabrication and characterization of PCL electrospun scaffolds – a review. J Mater Chem. 2011;21(26):9419–53.
45. Sant S, Hwang CM, Lee SH, Khademhosseini A. Hybrid PGS-PCL microfibrous scaffolds with improved mechanical and biological properties. J Tissue Eng Regen Med. 2011;5(4):283–91.
46. Nommeots-Nomm A, Hupa L, Rohanová D, Brauer DS. A review of acellular immersion tests on bioactive glasses—influence of medium on ion release and apatite formation. Int J Appl Glas Sci. 2020;11(3):537–51.
47. Kokubo T, Kushitani H, Sakka S, Kitsugi T, Yamamuro T. Solutions able to reproduce in vivo surface-structure changes in bioactive glass-ceramic A-W3. J Biomed Mater Res. 1990;24(6):721–34.
48. Maçon ALB, Kim TB, Valliant EM, Goetschius K, Brow RK, Day DE, et al. A unified in vitro evaluation for apatite-forming ability of bioactive glasses and their variants. J Mater Sci Mater Med. 2015;26(2):115.
49. Hench LL, West JK. Biological applications of bioactive glasses. Life Chem Rep. 1996;13:187–241.
50. Kim IY, Koichi K, Ohtsuki C. Hydroxyapatite formation through dissolution-precipitation reaction: Effects of solubility of starting materials. Ceram Int. 2014;40(9 PART A):14385–90.
51. Luginina M, Schuhladen K, Orrú R, Cao G, Boccaccini AR, Liverani L. Electrospun PCL/PGS composite fibers incorporating bioactive glass particles for soft tissue engineering applications. Nanomaterials. 2020;10(5):978.
52. Gómez-Lizárraga KK, Flores-Morales C, Del Prado-Audelo ML, Álvarez-Pérez MA, Piña-Barba MC, Escobedo C. Polycaprolactone- and polycaprolactone/ceramic-based 3D-bioplotted porous scaffolds for bone regeneration: a comparative study. Mater Sci Eng C. 2017;79:326–35.
53. Salehi S, Fathi M, Javanmard SH, Bahners T, Gutmann JS, Ergün S, et al. Generation of PGS/PCL blend nanofibrous scaffolds mimicking corneal stroma structure. Macromol Mater Eng. 2014;299(4):455–69.
54. Gaharwar AK, Nikkhah M, Sant S, Khademhosseini A. Anisotropic poly (glycerol sebacate)-poly (-caprolactone) electrospun fibers promote endothelial cell guidance. Biofabrication. 2015;7(1):15001.
55. Zheng K, Solodovnyk A, Li W, Goudouri O-M, Stähli C, Nazhat SN, et al. Aging time and temperature effects on the structure and bioactivity of gel-derived 45S5 glass-ceramics. J Am Ceram Soc. 2015;98(1):30–8.
56. Lázaro GS, Santos SC, Resende CX, dos Santos EA. Individual and combined effects of the elements Zn, Mg and Sr on the surface reactivity of a SiO_2·CaO·Na_2O·P_2O_5 bioglass system. J Non Cryst Solids. 2014;386:19–28.
57. Rabiee SM, Nazparvar N, Azizian M, Vashaee D, Tayebi L. Effect of ion substitution on properties of bioactive glasses: a review. Ceram Int. 2015;41(6):7241–51.
58. Atkinson I, Anghel EM, Predoana L, Mocioiu OC, Jecu L, Raut I, et al. Influence of ZnO addition on the structural, in vitro behavior and antimicrobial activity of sol–gel derived CaO–P_2O_5–SiO_2 bioactive glasses. Ceram Int. 2016;42(2):3033–45.
59. Shahrabi S, Hesaraki S, Moemeni S, Khorami M. Structural discrepancies and in vitro nanoapatite formation ability of sol-gel derived glasses doped with different bone stimulator ions. Ceram Int. 2011;37(7):2737–46.
60. Sánchez-Salcedo S, Shruti S, Salinas AJ, Malavasi G, Menabue L, Vallet-Regí M. In vitro antibacterial capacity and cytocompatibility of SiO_2-CaO-P_2O_5 meso-macroporous glass scaffolds enriched with ZnO. J Mater Chem B. 2014;2(30):4836–47.
61. Fiorio Pla A, Munaron L, Morterra C, Aina V, Malavasi G. Zinc-containing bioactive glasses: surface reactivity and behaviour towards endothelial cells. Acta Biomater. 2008;5(4):1211–22.
62. Haimi S, Gorianc G, Moimas L, Lindroos B, Huhtala H, Räty S, et al. Characterization of zinc-releasing three-dimensional bioactive glass scaffolds and their effect on human adipose stem cell proliferation and osteogenic differentiation. Acta Biomater. 2009;5(8):3122–31.
63. Li W, Zhou J, Xu Y. Study of the in vitro cytotoxicity testing of medical devices. Biomed Reports. 2015;3(5):617–20.
64. Wallin RF. A practical guide to ISO 10993–5: cytotoxicity a practical guide to ISO 10993–5. Cytotoxicity. 2015;10–3.
65. Mattila PK, Lappalainen P. Filopodia: molecular architecture and cellular functions. Nat Rev Mol Cell Biol. 2008;9(6):446–54.

How to cite this article: Neščáková Z, Kaňková H, Galusková D, Galusek D, Boccaccini AR, Liverani L. Polymer (PCL) fibers with Zn-doped mesoporous bioactive glass nanoparticles for tissue regeneration. Int J Appl Glass Sci. 2021;12:588–600. https://doi.org/10.1111/ijag.16292